Contrib Mineral Petrol (1996) 123:92–108

Keith Putirka · Marie Johnson · Rosamond Kinzler · John Longhi · David Walker

Thermobarometry of mafic igneous rocks based on clinopyroxene-liquid equilibria, 0–30 kbar

Received: 16 May 1994/Accepted: 15 June 1995

Abstract Models for estimating the pressure and temperature of igneous rocks from co-existing clinopyroxene and liquid compositions are calibrated from existing data and from new data obtained from experiments performed on several mafic bulk compositions (from 8–30 kbar and 1100–1475° C). The resulting geothermobarometers involve thermodynamic expressions that relate temperature and pressure to equilibrium constants. Specifically, the jadeite (Jd; $NaAlSi_2O_6$)–diopside/hedenbergite (DiHd; Ca(Mg, Fe)Si_2O_6) exchange equilibrium between clinopyroxene and liquid is temperature sensitive. When compositional corrections are made to the calibrated equilibrium constant the resulting geothermometer is

$$\text{(i)}\quad \frac{10^4}{T} = 6.73 - 0.26^{*}\ln\left[\frac{Jd^{px}{*}Ca^{liq}{*}Fm^{liq}}{DiHd^{px}{*}Na^{liq}{*}Al^{liq}}\right] - 0.86^{*}\ln\left[\frac{Mg^{liq}}{Mg^{liq}+Fe^{liq}}\right] + 0.52^{*}\ln[Ca^{liq}]$$

an expression which estimates temperature to $\pm$ 27 K. Compared to (i), the equilibrium constant for jadeite formation is more sensitive to pressure resulting in a thermobarometer

$$\text{(ii)}\quad P = -54.3 + 299^{*}\frac{T}{10^4} + 36.4^{*}\frac{T}{10^4}\ln\left[\frac{Jd^{px}}{[Si^{liq}]^2{*}Na^{liq}{*}Al^{liq}}\right] + 367^{*}[Na^{liq}{*}Al^{liq}]$$

which estimates pressure to $\pm$ 1.4 kbar. Pressure is in kbar, T is in Kelvin. Quantities such as Na^{liq} represent the cation fraction of the given oxide ($NaO_{0.5}$) in the liquid and Fm = MgO + FeO. The mole fractions of Jd and diopside + hedenbergite (DiHd) components are calculated from a normative scheme which assigns the lesser of Na or octahedral Al to form Jd; any excess Al^{VI} forms Calcium Tschermak's component (CaTs; $CaAlAlSiO_6$); Ca remaining after forming CaTs and $CaTiAl_2O_6$ is taken as DiHd. Experimental data not included in the regressions were used to test models (i) and (ii). Error on predictions of T using model (i) is $\pm$ 40 K. A pressure-dependent form of (i) reduces this error to $\pm$ 30 K. Using model (ii) to predict pressures, the error on mean values of 10 isobaric data sets (0–25 kbar, 118 data) is $\pm$ 0.3 kbar. Calculating thermodynamic properties from regression coefficients in (ii) gives V_f^{Jd} of 23.4 $\pm$ 1.3 cm^3/mol, close to the value anticipated from bar molar volume data (23.5 cm^3/mol). Applied to clinopyroxene phenocrysts from Mauna Kea, Hawaii lavas, the expressions estimate equilibration depths as great as 40 km. This result indicates that transport was sufficiently rapid that at least some phenocrysts had insufficient time to re-equilibrate at lower pressures.

K. Putirka (✉) · M. Johnson · R. Kinzler · J. Longhi · D. Walker
Lamont-Doherty Earth Observatory of Columbia University Palisades, NY 10964, USA

Editorial responsibility: T.L Grove

Overview

Thermobarometry applied to phenocrysts in volcanic rocks provides a method for determining depths and temperatures of magma storage. If magma stalls at the base of the crust prior to discharge, thermobarometry constrains crustal thickness, and perhaps also the geothermal gradient at the time of eruption. Few means of temperature estimation widely applicable to basaltic rocks exist and even fewer means of determining the pressures of phenocryst equilibration for such rocks currently exist. The thermobarometers presented here are calibrated using new experimental data and are based on clinopyroxene-liquid equilibria. Equilibria involving clinopyroxene were chosen for two reasons. (1) Clinopyroxene is a common phenocryst phase in

volcanic rocks; clinopyroxene-based thermobarometers will thus be of general applicability. (2) Formation of the clinopyroxene component jadeite is accompanied by a large change in molar volume and provides barometric information for igneous processes.

The thermobarometers are thermodynamic rather than empirical. They expand on the approaches taken by Roeder and Emslie (1970) and Drake (1976). Equilibrium constants (K_{eq}) describing pyroxene solution are calibrated for both pressure (P) and temperature (T). The advantage of calibrating equilibrium constants is that thermodynamic relationships exist which relate K_{eq} to T and P. A thermodynamic approach also allows extrapolation to pressures, temperatures, and compositions outside the experimental range used for calibration.

The large partial molar volumes for Na and Al oxides in basaltic liquid (Lange and Carmichael 1987) combined with the small partial molar volume of jadeite ($NaAlSi_2O_6$; Jd) result in a relatively large P-dependency for jadeite formation compared to other mineral-liquid equilibria (Table 1; see also Robie et al. 1979). The Jd-liquid equilibrium is also temperature-sensitive and is thus calibrated as a thermobarometer. The volume changes for the solution of Jd and calcium-Tschermak ($CaAlAlSiO_6$; CaTs) into diopside-hedenbergite ($Ca(Mg,Fe)Si_2O_6$; DiHd) are significantly smaller; these exchange-equilibria are temperature-dependent and are calibrated as thermometers. Both exchange equilibria, Jd-DiHd and CaTs-DiHd, require a pressure-dependent term for complete description. The thermometers are presented both with and without pressure terms; ignoring the pressure term facilitates application of the thermometers and results in only a slight increase in the uncertainty of the estimate.

As many of the pertinent thermodynamic data are lacking for the appropriate pyroxene and liquid components, the thermobarometers are constructed from regression analysis of experimental clinopyroxene-liquid equilibrium compositions. In an attempt to explore compositional complexities, new experiments were performed in the melting interval 8–30 kbar at 2 kbar intervals on a range of natural basalt compositions. Several solution models were tested. The resulting thermobarometers recover P and T for clinopyroxene-liquid pairs synthesized from other labs and yield thermodynamic quantities that compare well with known values.

It is unclear whether mafic volcanic rocks are erupted directly from substantial depths or are invariably processed in shallow-level magma reservoirs. Also uncertain is the depth of stagnation during different stages of volcanism; are the parental magmas of alkalic and tholeiitic suites extracted from different depths? Further, what controls depth of magma ponding: density contrasts or mechanical behavior of the lithosphere? These problems will be explored through application of the thermobarometers to pyroxene-bearing rocks from Mauna Kea, Hawaii.

Table 1 Thermodynamic properties[a]

Anticipated thermodynamic properties				
Equilibrium	ΔS^b	ΔS^c	ΔV^d_{1573}	ΔH^e_{1573}
Jd-liq	− 120	− 113	− 23.5	− 154
Di-Jd	56.7	47.1	− 10.8	− 7.7
Di-CaTs	54.0	–	− 1.33	–
Di-liq	− 63.3	− 65.9	–	− 146

Thermodynamic properties recovered from models				
K_{eq}	Model #	ΔS	ΔV	ΔH
Jd-liq	P1	− 71.6	− 23.2	− 128
Jd-liq	P2	− 95.6	− 23.4	− 129
Di-Jd	T1	193	–	288
Di-CaTs	T3	283	–	449

[a] Crystalline data are from Robie et al (1979); crystal molar volumes are corrected to 1573 K assuming $\alpha^{Jd} = 4.0 \times 10^{-5}$/K and $\alpha^{Di/CaTs} = 3.0 \times 10^{-5}$/K; ΔH is in kJ/mol, ΔS is in J/mol*K and volumes are cc/mol. SEE for model ΔH are $\pm$ 20 kJ/mol and for model $\Delta S \pm 5$ J/mol*K

[b] Calculation uses partial molar entropy of oxides at 298 K (Richet et al. 1993), integrated to 1600 K using partial molar C_p data from Stebbins et al. (1984) who determined C_p with data ranging from 1200–1850 K

[c] From C_p and S_{298}-S_0 data of jadeite and diopside glass reported by Richet et al. (1993, Table 7)

[d] Uses partial molar oxide data of Lange and Carmichael (1987)

[e] Derived from H_v and H_f data of Navrotsky (1981) and molar volume of jadeite glass (Richet et al. 1993); the estimate for H_f^{Jd} assumes that $H_{f,T_m}/H_{v,985}$ is the same for jadeite and diopside

Thermodynamic approach

Below we present the equilibria and thermodynamic equations used for thermobarometry. The thermodynamic database is presently inadequate to yield all the coefficients appearing in these equations. The following functions are thus used for regression analysis of experimental equilibrium clinopyroxene-liquid compositions.

As anticipated from existing molar volume data, a useful equilibrium for barometry involves jadeite formation (K[Jd-liq]). The exchange equilibria, diopside-jadeite (K[DiHd-Jd]), and diopside-calcium-Tschermak (K[DiHd-CaTs]), are less sensitive to P but are sensitive to T, providing pressure-sensitive thermometers. These equilibria may be expressed as

$$2SiO_2^{liq} + NaO_{1/2}^{liq} + AlO_{3/2}^{liq} = NaAlSi_2O_6^{px} \quad (1)$$

$$CaFmSi_2O_6^{px} + NaO_{1/2}^{liq} + AlO_{3/2}^{liq} = NaAlSi_2O_6^{px} + CaO^{liq} + FmO^{liq} \quad (2)$$

$$CaFmSi_2O_6^{px} + 2AlO_{3/2}^{liq} = CaAl^{VI}Al^{IV}SiO_6^{px} + FmO^{liq} + SiO_2^{liq} \quad (3)$$

where superscripts denote the phase (liq = liquid; px = pyroxene) and the symbol FmO refers to total (FeO + MgO). The methods used to calculate liquid and pyroxene components are discussed below.

As equilibrium constants will vary with P and T, expressions must be developed to quantify these dependencies. The relationship between K_{eq} and Gibbs free energy may be written as

$$-RT\ln K_{eq} = \Delta G_r^0 \tag{4}$$

where R is the gas constant, T is temperature (Kelvin) and ΔG_r^0 is the Gibbs free energy change for the stoichiometric equilibrium at a reference pressure P_0 and temperature, T. Rearranging and expanding ΔG_r^0 while holding ΔV_r constant yields

$$\ln K_{eq} = -\frac{\Delta H_r^{P_o}}{RT} + \frac{\Delta S_r^{P_o}}{R} - \frac{(P-P_0)\Delta V_r}{RT} \tag{5}$$

where $\Delta H_r^{P_o}$, ΔV_r, and $\Delta S_r^{P_o}$ are, respectively, the differences (products − reactants) of enthalpy, volume and entropy of a given equilibrium. Rearranging Eq. 5 to give P as the dependent variable gives

$$P = -\frac{RT}{\Delta V_r}\ln K_{eq} + \frac{\Delta S_r^{P_o}}{\Delta V_r}T - \frac{\Delta H_r^{P_o}}{\Delta V_r} \tag{6}$$

where $P_0 = 0$. Holding $\Delta H_r^{P_o}$, $\Delta S_r^{P_o}$ and ΔV_r constant, Eq. 6 provides the simplest function that satisfactorily describes variations in the experimental data. Temperature and pressure were measured directly in each experiment. K_{eq} is computed from microprobe analyses of coexisting pyroxenes and glass and is based on Equation 1, 2 or 3. The remaining quantities, $\Delta H_r^{P_o}$, $\Delta S_r^{P_o}$ and ΔV_r, are determined by regression analysis.

Equation 5 may be rearranged to give $1/T$ as the dependent variable,

$$\frac{1}{T} = -\frac{R}{(\Delta H_r^{P_o} + P\Delta V_r)}\ln K_{eq} + \frac{\Delta S_r^{P_o}}{(\Delta H_r^{P_o} + P\Delta V_r)} \tag{7}$$

If ΔV_r is zero (or if only data at $P = 0$ are utilized) then Eq. 7 reduces to

$$\frac{1}{T} = -\frac{R}{\Delta H_r^{P_o}}\ln K_{eq} + \frac{\Delta S_r^{P_o}}{\Delta H_r^{P_o}} \tag{8}$$

As with Eq. 6, the values for $R/\Delta H_r^{P_o}$ and $\Delta S_r^{P_o}/(\Delta H_r^{P_o})$ in Eq. 8 may be derived through regression analysis. Since Eq. 7 is not easily rearranged for $1/T$ with P and $\ln K_{eq}$ as separable, linear independent variables, the pressure dependency may be added to Eq. 8 empirically as:

$$\frac{1}{T} = -\frac{R}{\Delta H_r^{P_o}}\ln K_{eq} + \frac{\Delta S_r^{P_o}}{\Delta H_r^{P_o}} + A^*P \tag{9}$$

where the coefficient A is determined by multiple linear regression. Equation 9 is equivalent to Eq. 8 when $A = 0$.

Activity modifying terms

Mixing properties of pyroxene and liquid components are unlikely to be perfectly ideal; such non-idealities may reveal themselves as compositional dependencies residual from the T and P dependencies of K_{eq} anticipated from the equations presented above. To compensate for non-ideality and to produce expressions that are useful as geothermobarometers for natural systems, additional compositional terms were added to Eqs 6, 8 and 9. Compositional terms that most successfully improve regression statistics and the predictive power of the models are those that appear in the calibrated equilibria. Formally, equilibrium constants are the ratio of activities, a_i, (products divided by reactants) each raised to the power of the corresponding coefficient in a balanced chemical equilibrium. Equilibrium constants may be rewritten in terms of K_D where $K_{eq} = K_D K_\gamma$ and $a_i = X_i\gamma_i$. K_D is the ratio $\Pi X_i^{\propto}$ (prod)/$\Pi X_i^{\propto}$ (react), where X_i are mole fractions of components i, and the exponent $\propto$ represents the coefficient of i in a balanced chemical equilibrium. Similarly, K_γ is a ratio of activity-modifying constants, $\Pi_{\gamma_i}^{\propto}$ (prod)/$\Pi_{\gamma_i}^{\propto}$ (react).

Terms of the form $T\ln K_{eq}$ (Eq. 6) combine both temperature and implicit compositional information. Since $T\ln K_{eq} = T\ln(K_D K_\gamma) = T\ln K_D + T\ln K_\gamma$, any model regressed only with $T\ln K_D$ terms may appear to have non-ideal compositional dependencies upon the components appearing in the K_{eq}. If activity coefficients are known beforehand, Eq. 6 could be written as

$$P = -\frac{RT}{\Delta V_r}\ln K_D + \frac{\Delta S_r^{P_o}}{\Delta V_r}T - \frac{\Delta H_r^{P_o}}{\Delta V_r} - \frac{RT}{\Delta V_r}\ln K_\gamma \tag{10}$$

Note that the coefficients of $T\ln K_D$ and $T\ln K_\gamma$ are both $-R/\Delta V_r$. In the present case, however, the γ_i are unknown. Compositional dependencies may be written as terms of the type $(-R/\Delta V)\ T\ln K_\gamma = Y^*T\ln[\Pi X_i^{\propto}]$. The ΠX_i for any particular Y would include all components with the same activity coefficient (as, for example, appears to be the case for Na and Al) possibly reflecting coupling. Thus, for a single non-ideal component j, $(-R/\Delta V)\ T\ln K\gamma_j = Y^*T\ln[X_j^{\propto}]$ (let $\propto$ be positive or negative if j is on the products or reactants side respectively). Equation 10 in this case becomes,

$$P = -\frac{RT}{\Delta V_r}\ln K_D + \frac{\Delta S_r^{P_o}}{\Delta V_r}T - \frac{\Delta H_r^{P_o}}{\Delta V_r} - Y^*T\ln[\Pi X_i^{\propto}] \tag{11}$$

The γ_i may be determined by finding the value that $\Pi X_i^{\propto}$ must have so that Y has the value $-R/\Delta V_r$.

Equation 11 forms the basis of the 'activity-modifying' form of the thermobarometer (model P2). This procedure does not account for the P- or T-sensitivity of the activity coefficient and merely assumes that some number Y exists such that $\gamma_j = (X_j^{\propto})^Y$.

The compositional dependencies may be regressed as 'empirical' terms such as,

$$P = -\frac{RT}{\Delta V_r}\ln K_D + \frac{\Delta S_r^{P0}}{\Delta V_r}T - \frac{\Delta H_r^{P0}}{\Delta V_r} - C^*[\Pi X_i] \quad (12)$$

Equation 12 resembles Eq. 6, but with K_D replacing K_{eq} and ΠX_i as an added empirical parameter with corresponding coefficient C determined through regression (model P1). Note that exponents are assumed to be unity to simplify application. The thermodynamic interpretation of C in Eq. 12 is less clear than for Y in Eq. 11, but this form avoids introducing temperature a third time, facilitating $P - T$ estimates with minimal error when T is unknown. The right-most terms in Eqs. 11 and 12 may be repeated, as necessary, for all i components that have dissimilar activity coefficients. If two components are coupled (or have the same activity coefficients) then regression of the natural log of the terms individually would produce identical coefficients for each term, in which case they could then be combined. A similar approach to compositional dependencies was followed for the thermometric functions.

Experimental approach

Although many pyroxenes have been synthesized at high pressure, few studies have focused on growing pyroxenes from a single liquid composition over a wide pressure range. Further, many experiments have been geared toward understanding mid-ocean ridge magmatism and thus encompass a narrow range of starting compositions. As the goal of this study is to produce thermobarometers of general applicability, new experiments were performed to broaden the existing data base. These experiments were performed at temperatures at or near the pyroxene liquidus in order to maintain near-uniform liquid composition while varying P and T. Close attention was paid to determining equilibrium pyroxene and glass compositions. Some experimental modifications, discussed below, improved our ability to recover glass compositions unmodified by quench pyroxene overgrowths.

Experiments were run in Boyd-England piston-cylinder presses with a 1/2 inch bore. The pressure medium was $BaCO_3$ wrapped in Pb-foil. Samples were loaded into a graphite capsule surrounded by an alumina sleeve and situated between two Al_2O_3 end-plugs; these materials were placed within a graphite heater. Pressure was applied using the cold piston-in technique with a friction correction made for $BaCO_3$ (see Fram and Longhi, 1992). No pressure correction was made to the thermocouple emf. Temperatures were measured with type-D thermocouples (W + 3%Re/W + 25%Re). Thermal gradients across the sample are 5°C (Fram and Longhi 1992). Runs were performed at 2 to 3 kbar intervals between 8 and 30 kbar to establish clear trends with respect to pressure and K_{eq} for each bulk composition, and to provide numerical leverage for regression analysis. Experimental conditions and products are listed in Table 2. Run times vary from 1 to 6 days, most lasting 3 days. Volume percent liquid was determined optically; where reported as less than 100%, accuracy is ± 10%. Several runs crystallized garnet, olivine, orthopyroxene and/or plagioclase in addition to clinopyroxene. Many of the experiments performed by Walter and Presnall, whose (1994) data are incorporated into the models, are also multiply saturated. The presence of additional phases other than pyroxene and liquid should not affect the equilibria calibrated.

Experimental bulk compositions were selected to explore anticipated compositional dependencies (Table 3). The Woodlark Basin basalt is both Al_2O_3- and Na_2O-rich. A ugandite (a mafic, peralkaline volcanic rock) is low in SiO_2 and high in CaO, TiO_2, alkalis, and volatiles. An ankaramite (a mafic, pyroxene-phyric volcanic rock) is high in FeO + MgO and extends pyroxene-liquid equilibria to high pressures. A mid-ocean ridge basalt from the KANE Fracture Zone in the mid-Atlantic provides a less extreme, MgO-rich bulk composition. The basalts studied span a wide range of TiO_2, Cr_2O_3, and FeO contents. Since such elements may aid Na or Al substitution in pyroxene, they may affect the equilibria of Eqs. 1, 2 and 3. Phase equilibria data from experiments in the synthetic $SiO_2 + CaO + Al_2O_3 + MgO + Na_2O$ (SCAM + Na) system by Walter and Presnall (1994) provide a study of the equilibria in the absence of these elements.

Modifications to experimental procedure

Experiments performed at pressures above 12 kbar produced a noticeable quench crystalline phase along the crystal/liquid interface if quenched isobarically. This problem was minimized by employing the following modification. For experiments performed above 12 kbar, the pressure was dropped to 8–10 kbar immediately prior to shutting off the power. The entire procedure, dropping pressure then shutting off the power, takes 1–2 s. In experiments quenched in this manner, the quench phase is negligible (Fig. 1). Re-equilibration during quench could potentially cause crystal rims to re-melt. This is of critical concern since the rims are most likely to be in equilibrium with surrounding glass. Pyroxene dissolution rates are expected to be diffusion-controlled (Zhang et al. 1989) and for quench times of 1–2 sec the distance affected by dissolution both within the glass and crystal should be negligible. The diffusion coefficient of Al_2O_3 (D_{Al}) in liquid coexisting with diopside at 1375° C, 13 kbar is 7.3 μ^2/s (Zhang et al. 1989). The distance (d) through which the liquid is affected during a 2 s quench ($d = (D_{Al}t)^{1/2}$) is 3.8 μm. As a disturbance in liquid composition on this scale is not observed we conclude that resolution of pyroxene has not affected the interface composition. None of the crystals show significant melting and the glass in all experiments is homogeneous throughout the charge. The K_{eq} derived from such experiments also lie on trends continuous and overlapping with lower pressure experiments where the pressure-quench procedure was neither needed nor used.

This technique was found to suppress quench growth successfully in komatiitic melts, where the quench problem is otherwise most severe (Fig. 1). Cores and pistons also survived this procedure with no ill-effects. Figure 1A shows the pitfall of dropping the pressure too rapidly to 1 bar: the liquid in this case has expelled its volatiles. In some experiments disruption of the crystal pile took place and glass was preserved within crevasses. In experiment WB-17 (Fig. 1F) melt was injected within two halves of a broken garnet and small pyroxene crystals were swept into the crevasse.

Analytical procedure

Mineral and glass analyses were performed on a CAMECA MBX wavelength dispersive electron microprobe at Lamont-Doherty Earth Observatory (Table 4). The accelerating voltage was 15 kV and a 1–2 μm beam diameter was used. Counting times were 30 s and a PAP correction procedure was applied. Multiple analyses of a pyroxene standard (Kakanui) yield standard deviations of 0.17 wt% for all oxides except SiO_2, which has a standard deviation of

Table 2 Experimental conditions

Run #	P (kb)	T (K)	T (C)	Time (hours)	quench	Run Products	Percent liquid
A-11	8	1473	1200	67	T	cpx + ol + gl	90
A-3	8	1523	1250	67	T	gl	100
A-2	10	1573	1300	61	T	cpx + ol + gl	85
A-10	10	1598	1325	48	T	ol + gl	90
A-8	10	1623	1350	74.5	T	ol + gl	99
A-4	12	1593	1320	70	T	cpx + ol + gl	60
A-7	17	1643	1370	66	P	cpx + gl	60
A-6	20	1663	1390	24	P	cpx + gl	45
A-9	30	1748	1475	48	P	cpx + gar + gl	45
MA-9	8	1498	1225	94	T	cpx + gl	90
MA-5	8	1523	1250	72	T	gl	100
MA-8	10	1523	1250	73	T	cpx + gl	80
MA-6	10	1543	1270	72	T	cpx + gl	90
MA-11	12	1548	1275	63	T	cpx + plag + gl	70
MA-10	15	1573	1300	93	T	cpx + gl + pl	60
MA-12	20	1613	1340	96	T	gar + cpx + gl	55
WB-13	8	1473	1200	72	T	cpx + gl	95
WB-15	10	1373	1100	166	T	cpx + opx + gl	10
WB-7	10	1498	1225	120	T	gl	100
WB-21	12	1498	1225	72	T	cpx + gl	80
WB-9	12	1498	1225	67	T	cpx + gl	80
WB-17	15	1423	1150	95	P	cpx + gar + gl	55
WB-14	15	1473	1200	73	P	cpx + gar + gl	70
WB-11	15	1513	1240	46	T	cpx + gl	80
WB-18	20	1573	1300	70	P	cpx + gar + gl	85
WB-20	25	1623	1350	72	T	gar + gl	90
U-1	8	1423	1150	46	T	cpx + gl	85
U-2	10	1443	1170	48	T	cpx + gl	90
U-3	12	1473	1200	49	T	cpx + gl	90
U-4	15	1498	1225	70	T	cpx + gl	90
U-5	20	1543	1270	70	P	cpx + gl	85

Quench: 'T' refers to experiments quenched at indicated pressure by shutting off power. 'P' refers to experiments where pressure was dropped prior to power shut-off

Table 3 Starting compositions (wt%)

Sample	SiO_2	TiO_2	Al_2O_3	FeO	MnO	MgO	CaO	Na_2O	K_2O	Cr_2O_3	total
MAR Basalt[a]	49.79	1.38	15.92	9.38	0.18	8.88	11.28	3.00	0.11	0.00	99.92
Woodlark Basin Basalt[b]	48.26	2.31	16.97	10.02	0.13	6.47	9.78	5.08	0.09	0.02	99.11
Ugandite[c]	36.85	6.09	9.83	13.74	0.26	5.53	13.52	2.51	6.13	0.01	94.47
Ankaramite[d]	47.85	3.16	11.76	13.14	0.21	10.55	10.03	2.20	0.65	0.10	99.55

[a] Mid-Atlantic Ridge Basalt (near Kane Fracture Zone) donated by Jennifer Reynolds
[b] Woodlark Basin Basalt = sample G32-8 from Perfit et al. (1987)
[c] Ugandite donated by Richard Sack
[d] Ankaramite = sample LP-5 from Frey et al. (1991)

0.42. Alkali-loss was minimized by first determining Na_2O and K_2O at 5 nA, then determining all other elements at 25 nA. Glass analyses are homogeneous throughout each charge. Pyroxenes, however, are not. Many experiments show thermal compaction of crystalline material at the cold end of the capsule. Crystals far from the crystal/liquid interface have variable composition and were deemed unlikely to be in equilibrium with the melt. Intracrystalline variation also occurs at the interface but core-to-rim variations are not systematic. For a given experiment, the most consistent pyroxene analyses are from rim compositions of crystals next to the crystal/liquid interface. Selecting analyses in this manner is necessary when the closest possible approach to equilibrium crystal compositions in crystallization experiments is required.

Data sets of other studies

Although no systematic study has been previously performed involving the pressure-sensitivity of pyroxene-liquid equilibria, pyroxene-liquid pairs from existing experimental work are available. These data allow an independent test of the thermobarometric models derived from the data of this study.

Several caveats must accompany the use of previously published data. (1) Although many published studies show general trends of increasing Al- and Na-contents of pyroxene as pressure increases, only in the Walter and Presnall (1994) data set were the analytical procedures outlined above ostensibly followed. (2) For runs at high pressure (> 12 kbar), if an isobaric quench procedure was followed,

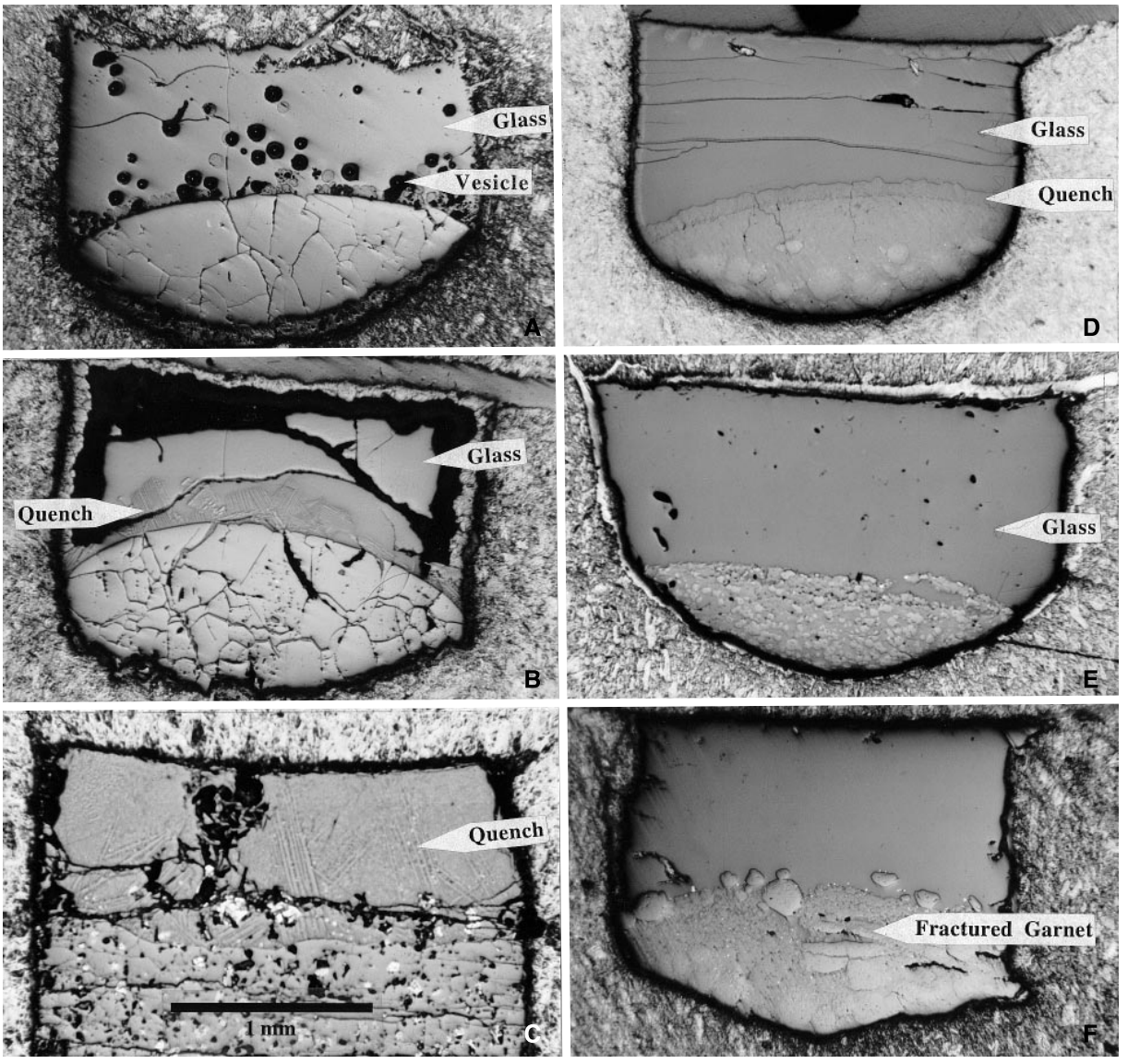

Fig. 1A and **B** show the effect of reducing pressure on komatiite bulk compositions just prior to thermal quench (scale in **C**). In **A** the pressure was dropped (accidentally) to 1 bar; note the vesicles. In **B** the pressure was dropped to the target pressure of 8 kbar; the entire upper portion of the charge recovered glass with relatively little crystalline quench. A "normal", thermal quench performed on a chondrite bulk composition is shown in **C** for comparison. **D** and **E** compare the effects of thermal and pressure quench procedures on basalt compositions. **D** is run# MA-12 where a thermal quench procedure was used; note the rim of quench growth separating pyroxenes from glass. **E** is run# WB-18 where a pressure quench procedure was used; note the absence of quench and also the disruption of the crystal pile. **F** is run# WB-17, also pressure-quenched. This sample shows a garnet crystal that was split. Melt was injected into the crevasse carrying with it several small pyroxene crystals. See text for description of the procedure

the presence of a quench phase may have hindered determining the equilibrium glass and pyroxene-rim compositions. (3) For 1 bar experiments, possible Na-loss from the melt during the experiment (Tormey et al. 1987) may lead to spuriously high K_{eq} for the equilibria of Eqs. 1 and 2.

Component calculations and experimental clinopyroxene compositions

As all models are based on equilibrium constants, appropriate components for the liquid and clinopyroxene phases must be chosen. Pyroxene components were initially assumed to be ideal ($a_i = X_i$). Although clearly incorrect, abandoning this assumption led to little improvement in the models. Liquid components were ultimately computed as a cation fraction. Ideal mixing of oxides in the liquid was also used as a starting point in calculating K_{eq}. Compositional terms were added if they improved both the quality of regression statistics and predictive power of the models. Interpretation of these compositional terms is given in the Activity-modifying Terms section.

Pyroxene cations are calculated per 6 oxygens. The Jd component is the amount of Na or octahedral Al ($Al^{VI} = Al^{tot} - Al^{IV}$; $Al^{IV} = 2 - Si$), whichever is less. The CaTs component is equal to any remaining Al^{VI}($CaTs = Al^{VI} - Jd$). Al^{IV} in excess of that required to form CaTs is used to form $CaTiAl_2O_6$ ($CaTiAl_2O_6 = [Al^{IV} - CaTs]/2$). Where there is insufficient Al^{VI} to form CaTs, the CaTs component is set to zero. Calcium remaining after forming CaTs and $CaTiAl_2O_6$ (CaTi) gives the $CaFmSi_2O_6$

Table 4 Compositions of pyroxenes and coexisting glass (wt %, NA not analyzed, standard deviations in italics)

Run #	P (kb)	T (C)	phase	SiO_2	TiO_2	Al_2O_3	FeO	MnO	MgO	CaO	Na_2O	K_2O	Cr_2O_3	Total	# Avgd
MAR-(Kane Fracture Zone) Data															
MA-9	8	1225	pyx	49.94	0.91	7.96	6.90	0.17	16.80	16.93	0.51	0.02	0.16	100.30	2
				0.86	*0.02*	*0.80*	*0.31*	*0.02*	*1.19*	*0.98*	*0.07*	*0.01*	*0.04*		
			gl	49.95	1.48	17.78	10.33	0.18	7.11	9.89	3.06	0.14	0.02	99.94	5
				0.26	*0.02*	*0.16*	*0.09*	*0.02*	*0.18*	*0.11*	*0.09*	*0.02*	*0.02*		
MA-8	10	1250	pyx	49.85	0.69	8.40	6.37	0.15	16.09	17.39	0.66	0.00	0.24	99.84	4
				0.62	*0.05*	*0.58*	*0.20*	*0.01*	*0.56*	*0.28*	*0.04*	*0.01*	*0.04*		
			gl	49.76	1.50	17.27	10.26	0.17	7.36	10.00	3.08	0.10	0.00	99.50	3
				0.19	*0.00*	*0.07*	*0.05*	*0.02*	*0.30*	*0.09*	*0.03*	*0.01*	*0.01*		
MA-6	10	1270	pyx	50.17	0.88	9.08	7.78	0.14	15.44	15.86	0.63	0.00	0.08	100.05	2
				0.36	*0.02*	*0.10*	*0.77*	*0.02*	*1.15*	*1.14*	*0.05*	*0.01*	*NA*		
			gl	49.90	1.59	17.16	10.31	0.16	7.21	9.95	2.95	0.12	0.01	99.37	3
				0.12	*0.03*	*0.17*	*0.06*	*0.02*	*0.07*	*0.06*	*0.19*	*0.01*	*NA*		
MA-11	12	1275	pyx	48.66	1.19	10.45	9.29	0.22	14.57	15.26	0.87	0.02	0.06	100.60	1
				NA	*NA*	*NA*	*NA*	*NA*	*NA*	*NA*	*NA*	*NA*	*NA*		
			gl	49.84	1.58	18.06	10.70	0.19	6.76	9.41	3.19	0.16	0.03	99.91	4
				0.10	*0.02*	*0.03*	*0.08*	*0.02*	*0.01*	*0.06*	*0.05*	*0.01*	*0.02*		
MA-10	15	1300	pyx	49.16	0.71	10.35	6.59	0.14	14.36	16.99	1.00	0.01	0.14	99.46	5
				0.65	*0.03*	*0.15*	*0.28*	*0.02*	*0.17*	*0.47*	*0.09*	*0.00*	*0.02*		
			gl	49.11	1.63	17.69	10.77	0.18	6.51	9.08	3.60	0.16	0.01	98.74	4
				0.33	*0.02*	*0.11*	*0.05*	*0.02*	*0.06*	*0.10*	*0.06*	*0.04*	*0.01*		
MA-12	20	1340	pyx	50.12	0.61	11.17	6.19	0.13	13.06	17.13	1.57	0.01	0.17	100.16	4
				0.54	*0.13*	*0.24*	*0.43*	*0.02*	*0.08*	*0.52*	*0.04*	*0.01*	*0.01*		
			gl	49.55	1.66	17.46	10.44	0.17	6.48	9.29	3.46	0.17	0.02	98.69	4
				0.14	*0.04*	*0.08*	*0.06*	*0.03*	*0.04*	*0.06*	*0.09*	*0.03*	*0.02*		
Woodlark Basin Data															
WB-13	8	1200	pyx	51.01	0.95	5.43	6.59	0.21	17.68	17.78	0.72	0.00	0.21	100.58	3
				0.37	*0.21*	*0.49*	*0.17*	*0.03*	*0.32*	*0.12*	*0.04*	*0.01*	*0.03*		
			gl	46.89	2.37	17.26	10.32	0.18	6.88	8.76	4.30	0.08	0.02	97.07	3
				0.43	*0.10*	*0.14*	*0.14*	*0.01*	*0.02*	*0.12*	*0.07*	*0.16*	*0.03*		
WB-15	10	1100	pyx	48.99	1.63	8.63	10.58	0.24	13.16	16.06	0.87	0.00	NA	100.17	2
				0.15	*0.15*	*0.22*	*0.05*	*0.04*	*0.10*	*0.21*	*0.02*	*0.00*	*NA*		
			gl	50.82	2.24	19.34	11.09	0.19	3.78	6.41	5.60	0.12	NA	99.60	4
				0.26	*0.02*	*0.09*	*0.07*	*0.02*	*0.07*	*0.05*	*0.15*	*0.03*	*NA*		
WB-21	12	1225	pyx	48.09	1.44	9.10	7.16	0.20	15.50	17.10	0.86	0.03	0.11	99.58	3
				0.29	*0.09*	*0.41*	*0.51*	*0.02*	*0.56*	*0.50*	*0.03*	*0.01*	*0.02*		
			gl	47.94	2.55	19.23	11.08	0.16	6.52	7.96	4.51	0.08	0.02	100.04	4
				0.85	*0.05*	*0.13*	*0.10*	*0.02*	*0.04*	*0.06*	*0.08*	*0.01*	*0.01*		
WB-9	12	1225	pyx	49.70	1.12	8.38	6.52	0.16	14.66	17.85	0.98	0.01	NA	99.38	3
				0.10	*0.06*	*0.47*	*0.25*	*0.03*	*0.31*	*0.35*	*0.07*	*0.01*	*NA*		
			gl	47.17	2.53	18.02	10.47	0.18	6.37	8.43	3.77	0.11	NA	97.03	3
				0.45	*0.00*	*0.05*	*0.07*	*0.01*	*0.08*	*0.03*	*0.09*	*0.02*	*NA*		
WB-17	15	1150	pyx	48.81	1.66	10.50	7.20	0.18	12.41	18.22	1.72	0.02	0.12	100.84	2
				0.10	*0.06*	*0.17*	*0.15*	*0.01*	*0.05*	*0.13*	*0.02*	*0.01*	*0.00*		
			gl	49.70	2.79	18.72	10.20	0.16	5.07	7.00	3.58	0.11	0.03	97.35	2
				0.94	*0.22*	*0.58*	*0.14*	*0.06*	*0.52*	*0.02*	*0.10*	*0.03*	*0.02*		
WB-11	15	1240	pyx	48.11	1.39	10.30	7.23	0.19	13.66	17.15	1.34	0.00	0.14	99.52	3
				0.32	*0.32*	*0.28*	*0.18*	*0.01*	*0.42*	*0.16*	*0.16*	*0.00*	*0.02*		
			gl	47.15	2.64	18.24	10.84	0.15	6.43	8.08	4.19	0.10	0.00	97.81	2
				0.25	*0.01*	*0.08*	*0.16*	*0.00*	*0.00*	*0.01*	*0.00*	*0.02*	*0.00*		
WB-14	15	1200	pyx	49.25	1.37	10.78	6.95	0.07	12.89	17.12	1.50	0.01	0.07	100.00	7
				0.31	*0.10*	*0.25*	*0.26*	*0.07*	*0.25*	*0.48*	*0.06*	*0.01*	*0.03*		
			gl	49.22	2.78	18.15	9.98	0.14	5.21	7.78	4.17	0.08	NA	97.50	4
				0.32	*0.02*	*0.18*	*0.11*	*0.02*	*0.03*	*0.06*	*0.05*	*0.01*	*NA*		
WB-18	20	1300	pyx	50.98	0.96	10.50	5.90	0.11	12.23	17.80	1.82	0.03	0.10	100.41	2
				0.59	*0.01*	*0.00*	*0.01*	*0.02*	*0.09*	*0.00*	*0.25*	*0.02*	*0.01*		
			gl	48.34	2.43	16.70	10.36	0.18	7.23	8.90	3.86	0.07	0.03	98.10	3
				0.37	*0.09*	*0.78*	*0.33*	*0.02*	*0.32*	*0.34*	*0.15*	*0.02*	*0.03*		
Ankaramite Data															
A-11	8	1200	pyx	50.64	1.33	5.86	10.77	0.19	17.63	13.52	0.54	0.02	0.23	100.49	4
				0.56	*0.19*	*0.80*	*0.58*	*0.03*	*0.36*	*0.93*	*0.07*	*0.02*	*0.04*		
			gl	46.67	4.34	16.08	14.20	0.17	6.27	8.08	3.29	1.20	0.01	100.31	5
				0.20	*0.03*	*0.11*	*0.09*	*0.03*	*0.06*	*0.04*	*0.06*	*0.03*	*0.02*		

Table 4 Continued

Run #	P (kb)	T (C)	phase	SiO_2	TiO_2	Al_2O_3	FeO	MnO	MgO	CaO	Na_2O	K_2O	Cr_2O_3	Total	# Avgd
A-2	10	1300	pyx	52.65	0.71	4.09	8.84	0.18	20.72	12.01	0.50	0.02	0.45	99.70	3
				0.19	*0.03*	*0.28*	*0.17*	*0.02*	*0.60*	*0.49*	*0.03*	*0.02*	*0.09*		
			gl	46.59	3.54	13.55	13.38	0.20	8.90	9.46	2.76	0.86	0.07	99.31	3
				0.31	*0.01*	*0.11*	*0.24*	*0.01*	*0.32*	*0.14*	*0.08*	*0.03*	*0.01*		
A-4	12	1320	pyx	51.58	0.85	5.17	9.10	0.17	19.20	12.80	0.71	0.01	0.27	99.58	4
				0.36	*0.08*	*0.20*	*0.14*	*0.02*	*0.41*	*0.63*	*0.06*	*0.02*	*0.02*		
			gl	45.06	3.82	13.39	14.36	0.18	8.98	8.72	3.16	0.92	0.04	98.62	4
				0.39	*0.06*	*0.11*	*0.08*	*0.01*	*0.06*	*0.04*	*0.07*	*0.05*	*0.02*		
A-7	17	1370	pyx	50.82	0.77	5.77	10.23	0.20	20.91	10.06	0.90	0.04	0.23	99.66	5
				1.02	*0.22*	*0.56*	*0.34*	*0.02*	*0.76*	*0.69*	*0.09*	*0.05*	*0.03*		
			gl	44.16	4.11	12.83	14.99	0.18	10.14	8.62	2.80	1.03	0.04	98.90	4
				0.20	*0.02*	*0.04*	*0.35*	*0.03*	*0.25*	*0.03*	*0.04*	*0.04*	*0.02*		
A-6	20	1390	pyx	51.49	0.75	7.16	9.54	0.17	18.52	11.41	1.07	0.01	0.27	100.11	5
				0.44	*0.10*	*0.45*	*0.14*	*0.02*	*0.57*	*0.58*	*0.14*	*0.01*	*0.06*		
			gl	45.86	3.93	13.25	15.00	0.18	9.76	8.71	2.45	0.94	0.05	100.14	4
				0.22	*0.06*	*0.13*	*0.43*	*0.02*	*0.08*	*0.22*	*0.40*	*0.11*	*0.03*		
A-9	30	1475	pyx	52.50	0.77	8.15	9.01	0.17	15.81	12.36	1.76	0.02	0.19	100.53	5
				0.36	*0.04*	*0.14*	*0.04*	*0.02*	*0.18*	*0.25*	*0.14*	*0.02*	*0.02*		
			gl	45.38	4.49	11.60	15.14	0.18	8.88	8.53	2.57	1.14	0.03	97.94	3
				0.27	*0.03*	*0.13*	*0.30*	*0.02*	*0.16*	*0.09*	*0.05*	*0.01*	*0.02*		
Ugandite Data															
U-1	8	1150	pyx	49.66	2.66	4.42	5.58	0.10	13.53	23.59	0.36	0.05	0.03	99.98	4
				0.55	*0.31*	*0.36*	*0.25*	*0.05*	*0.31*	*0.19*	*0.05*	*0.05*	*0.01*		
			gl	36.91	6.13	10.07	13.83	0.25	5.41	13.35	2.53	6.30	0.00	94.79	3
				0.29	*0.09*	*0.10*	*0.26*	*0.03*	*0.09*	*0.13*	*0.20*	*0.11*	*0.00*		
U-2	10	1170	pyx	49.46	2.30	4.29	5.57	0.16	13.90	23.56	0.39	0.01	0.00	99.64	2
				0.03	*0.10*	*0.27*	*0.07*	*0.02*	*0.51*	*0.14*	*0.03*	*0.02*	*0.00*		
			gl	36.81	6.18	9.98	13.38	0.27	5.45	13.42	2.49	6.05	0.01	94.03	3
				0.06	*0.01*	*0.03*	*0.22*	*0.03*	*0.04*	*0.06*	*0.08*	*0.13*	*0.01*		
U-3	12	1200	pyx	51.33	2.16	4.69	5.56	0.12	13.22	23.41	0.49	0.03	0.05	101.06	3
				0.68	*0.20*	*0.24*	*0.23*	*0.01*	*0.15*	*0.07*	*0.09*	*0.01*	*0.01*		
			gl	36.80	5.94	9.68	13.24	0.26	5.51	13.60	2.55	5.94	0.01	93.54	3
				0.25	*0.02*	*0.09*	*0.14*	*0.02*	*0.02*	*0.19*	*0.17*	*0.02*	*0.01*		
U-4	15	1225	pyx	48.91	2.24	6.13	6.24	0.11	12.51	22.93	0.55	0.04	0.01	99.67	3
				0.92	*0.19*	*0.55*	*0.06*	*0.01*	*0.24*	*0.27*	*0.03*	*0.01*	*0.01*		
			gl	36.94	6.15	9.84	14.60	0.24	5.64	13.54	2.48	6.41	0.02	95.87	4
				0.10	*0.00*	*0.09*	*0.23*	*0.02*	*0.06*	*0.07*	*0.05*	*0.13*	*0.03*		
U-5	20	1270	pyx	47.02	2.90	8.65	6.85	0.11	11.62	22.07	0.86	0.64	0.00	100.71	3
				0.21	*0.19*	*0.22*	*0.28*	*0.03*	*0.18*	*0.11*	*0.03*	*0.00*	*0.00*		
			gl	37.21	5.79	9.59	13.89	0.26	5.49	13.52	2.65	6.63	0.02	95.06	2
				0.99	*0.31*	*0.40*	*0.26*	*0.01*	*0.50*	*0.28*	*0.00*	*0.41*	*0.03*		

(DiHd) component (DiHd = Ca − CaTs–CaTi). The enstatite-ferrosilite (EnFs) component is equal to one-half the Fm component remaining after forming DiHd (EnFs = [Fm-DiHd]/2). If the calculation is performed correctly and the cation sum is four, the pyroxene components in this scheme should sum to unity (see also Lindsley (1983), for calculation of pyroxene components). In calculating K_{eq} pyroxene component activities are set equal to the amounts calculated from the normative procedure.

Titanium contents of experimental pyroxenes have a one-to-one correlation with CaTi components as calculated above (Ti vs CaTi has a slope of one, an intercept of zero and R = 0.88). This correlation indicates a coupled substitution of the type $TiAl_2(MSi_2)_{-1}$ where M is a divalent cation (Sack and Carmichael 1984; Gee and Sack 1988). Experimental pyroxenes contain very little Cr and the thermobarometers predict the test data best when no attempt is made to account for a Cr-component in pyroxene. Pyroxenes were also analyzed for Mn and K; these elements were not used in calculating pyroxene components. Since all experiments were performed in graphite capsules the acmite ($NaFe^{3+}Si_2O_6$)component was considered negligible; this expectation was borne out by charge balance calculations (Lindsley 1983) that revealed minimal Fe^{3+} in pyroxene. All pyroxenes of this study and in Walter and Presnall (1994) contain sufficient Al to form a CaTs component. As might be expected for pyroxenes in the SCAM + Na system, no significant Al^{IV} in excess of CaTs exists; Al^{IV} and CaTs are highly correlated (Al^{IV} vs CaTs has a slope of 0.9, an intercept of 0, and R = 0.97) indicating that charge balance for Al^{IV} in the tetrahedral site is taken up by Al^{VI} rather than vacancies.

Results

Thermobarometers employing various activity models (Ghiorso et al. 1983; Nielsen and Drake 1979; simple cation fraction), compositional corrections and variations on the expansion of Eq. 4, were initially ranked on the basis of regression statistics. Models were then compared and tested on their ability to predict *P* and

T from the test data. The test data set comprises 129 experimental pyroxene/glass pairs synthesized from 1 bar to 50 kbar. Sources for test data are listed in the appropriate figure captions. Satisfactory thermobarometers were constructed from regressions based only on the data of Table 4 and from Walter and Presnall (1994) and thus do not include any 1 bar data. Thermometric functions, however, were greatly improved when randomly selected 1 bar data were incorporated into the regressions. All 1 bar data incorporated into the thermometers for regression analysis were removed from the data set used to test the thermometers, thus avoiding overlap between test and regression data sets. As a final consistency check for the thermobarometers, thermodynamic quantities were computed from regression coefficients and compared to existing (1 bar) thermodynamic data.

We observed that use of liquid components expressed as a cation fraction led to the most successful thermobarometers and thermometers. The thermobarometers are presented in two forms (Table 5): P1 presents compositional dependencies in their 'empirical' form as shown in Eq. 12, while model P2 uses the explicit activity-modifying form of Eq. 11. The product, $Na^{liq}*Al^{liq}$, (models P1 and P2) implies identical activity coefficients for Na^{liq} and Al^{liq}. Nielsen and Drake (1979), motivated by the work of Bottinga and Weill (1972), found that combining Na- and Al-activities as an $NaAlO_2^{liq}$ component was useful in describing 1 bar pyroxene-liquid equilibria. Application of their silicate melt activity model was, however, less successful than simple cation units in predicting test data.

Thermobarometers

On the basis of regression statistics, slope and intercept values of predicted vs measured P, and prediction of test data, model P1 is our preferred model for P estimation. Model P1 yields the lowest standard error of estimate (SEE) of all thermobarometers tested. The SEE represents the formal error of a model and is analogous to the standard deviation of a mean. In the present context, it is the number E for which the probability is 68% that any individual P (or T) estimate is within $\pm$ E of the true (model) value. If errors in pressure, temperature and compositional measurements are random, the mean of predictions of a set of isobaric experiments should be normally distributed about the reported value. Error from any other well-characterized set of equilibrium pyroxene-glass pairs with similar analytical and experimental uncertainty should be comparable to the model SEE.

8–50 kbar

Predictions of models P1 and P2 against the regression data are shown Fig. 2. Figures 3 and 4 show how well these models predict the test data. Model P1, employing the empirical form of the compositional term $Na^{liq}*Al^{liq}$, predicts P somewhat better than model P2 (SEE = 1.36 vs 1.51 kbar). The lower apparent accuracy of model P2 may result from error added by introducing temperature a third time (in the

Table 5 Thermobarometers (T in units of Kelvin, P in kbar, *Fm* FeO + MgO, *DiHd* Di + Hd; superscripts denote phase—*px* pyroxene, *liq* liquid; liquid components in cation fraction; see text for calculation of pyroxene components)

Thermobarometric models

P1
$$P = -54.3 + 299\frac{T}{10^4} + 36.4\frac{T}{10^4}\ln\left[\frac{Jd^{px}}{[Si^{liq}]^2*Na^{liq}*Al^{liq}}\right] + 367\,[Na^{liq}*Al^{liq}]$$

P2
$$P = -50.7 + 394\frac{T}{10^4} + 36.4\frac{T}{10^4}\ln\left[\frac{Jd^{px}}{[Si^{liq}]^2*Na^{liq}*Al^{liq}}\right] - 20.0\frac{T}{10^4}\ln\left[\frac{1}{[Na^{liq}*Al^{liq}]}\right]$$

Thermometric models

T1
$$\frac{10^4}{T} = 6.73 - 0.26*\ln\left[\frac{Jd^{px}*Ca^{liq}*Fm^{liq}}{DiHd^{px}*Na^{liq}*Al^{liq}}\right] - 0.86*\ln\left[\frac{Mg^{liq}}{Mg^{liq}+Fe^{liq}}\right] + 0.52*\ln[Ca^{liq}]$$

T2
$$\frac{10^4}{T} = 6.59 - 0.16*\ln\left[\frac{Jd^{px}*Ca^{liq}*Fm^{liq}}{DiHd^{px}*Na^{liq}*Al^{liq}}\right] - 0.65*\ln\left[\frac{Mg^{liq}}{Mg^{liq}+Fe^{liq}}\right] + 0.23*\ln[Ca^{liq}] - 0.02p$$

T3
$$\frac{10^4}{T} = 6.92 - 0.18*\ln\left[\frac{CaTs^{px}*Si^{liq}*Fm^{liq}}{DiHd^{px}*[Al^{liq}]^2}\right] - 0.84*\ln\left[\frac{Mg^{liq}}{Mg^{liq}+Fe^{liq}}\right] - 0.29*\ln\left[\frac{1}{[Al^{liq}]^2}\right]$$

T4
$$\frac{10^4}{T} = 7.20 - 0.04*\ln\left[\frac{CaTs^{px}*Si^{liq}*Fm^{liq}}{DiHd^{px}*[Al^{liq}]^2}\right] - 0.59*\ln\left[\frac{Mg^{liq}}{Mg^{liq}+Fe^{liq}}\right] - 0.18*\ln\left[\frac{1}{[Al^{liq}]^2}\right] - .03*P$$

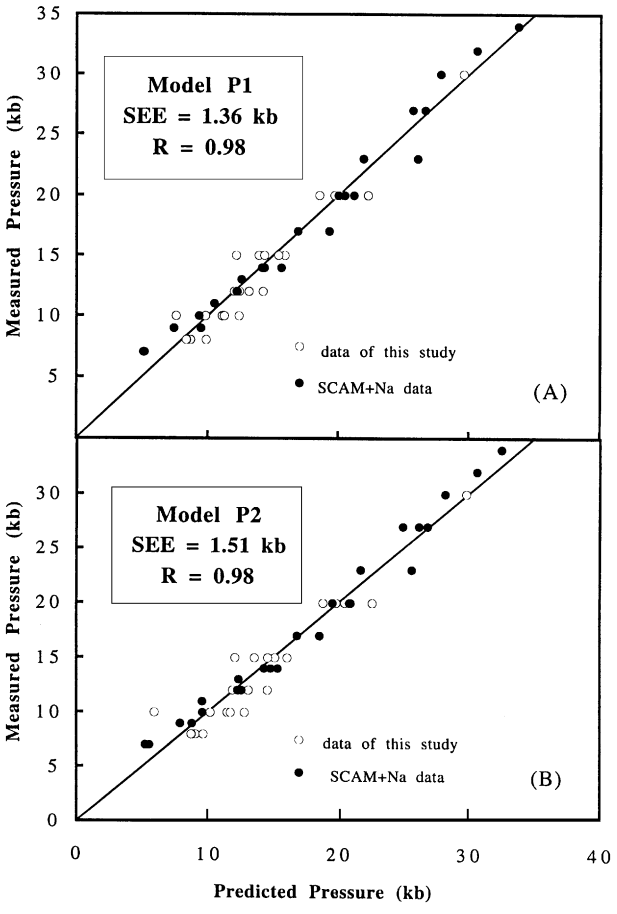

Fig. 2 Models P1 **A** and P2 **B** are used to recover pressures for the data used in the regressions. The lines shown are one-to-one correlation lines. The statistics in each figure are for regressions on the model data

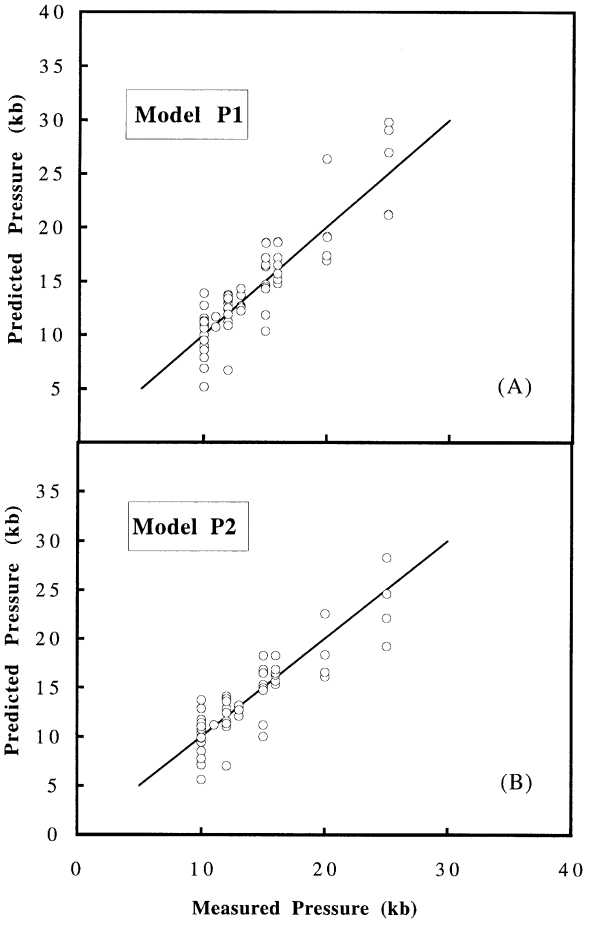

Fig. 3 Models P1 **A** and P2 **B** are used to predict pressures from published experimental data (data not used in the regressions) from 8 to 25 kbar. The lines shown are one-to-one correlation lines. The data are from Bartels et al. (1991), Elthon and Scarfe (1984), Falloon and Green (1987), and Kinzler and Grove (1992). Also included are unpublished data from John Longhi and Rosamond Kinzler

activity-modifying parameter). Model P1 is thus recommended for $P - T$ estimates of natural samples.

The mean values of predicted pressures using model P1 for data in the 8–25 kbar range match the measured values with a SEE of 0.3 kbar (Fig. 4A). Takahashi's (1986) 50 kbar experiment provides the only clinopyroxene-liquid pair synthesized from a mafic bulk composition at a significantly greater pressure than those used for calibration. The model recovers a pressure of 50 kbar indicating that model P1 may extrapolate to pressures higher than the *P*-range of the regression data.

Standard deviations for the 20 and 25 kbar portion of the test data set are large compared to other pressures. These data comprise experiments performed on lunar analogs (John Longhi, unpublished data) and oceanic basalts (Elthon and Scarfe 1984). In the first study two runs at 20 and 25 kbar respectively with very FeO-rich (33 and 27 wt%) and SiO_2-poor (36 and 34 wt%) liquids yield erroneously high pressures, indicating that the model may not extrapolate to these compositions. Also, predictions based on Elthon and Scarfe data are consistently low by 3–4 kbar. Run durations were very short for these experiments (1 h) and equilibrium may not have been achieved. Because the 20–25 kbar portion of the test data set is small, statistics on mean values are also reported for the 1 bar–16 kbar portion of the test data set in the appropriate figure captions.

To understand the uncertainty in $P - T$ estimates of natural samples it is necessary to understand the sources of model error. Interlab pressure-calibration problems, if systematic, might contribute to model inaccuracy. The models are based on data from two different laboratories using different pressure calibration procedures (piston-in at LDEO vs piston-out at UTD) and yet the data regress well together. Furthermore, test data from Kinzler and Grove (1992) fall within the SEE of the models. At least for these three data sets little indication exists of a substantial *P*

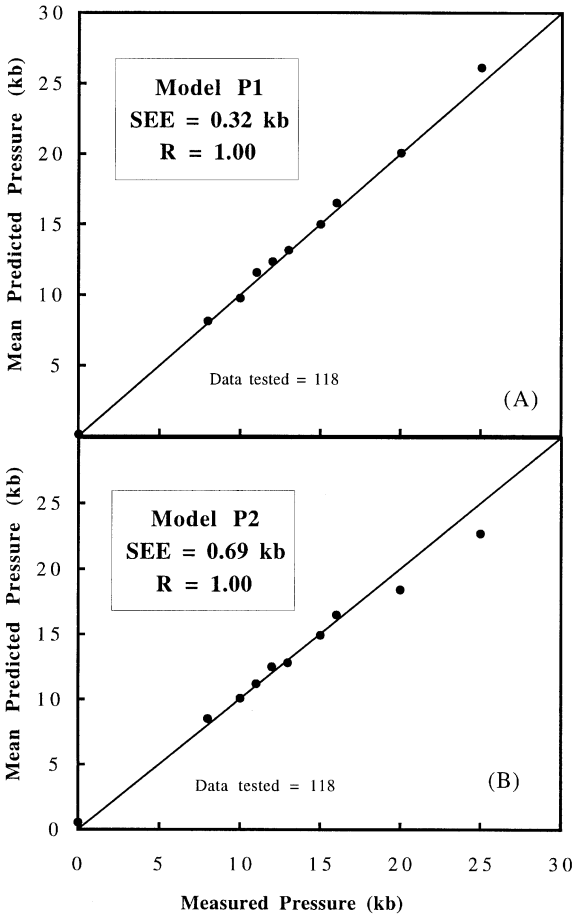

Fig. 4A, B The isobaric means of the predicted pressures of data shown in Fig. 3**A** and **B** are plotted against measured pressure. **A** and **B** correspond to models P1 and P2 respectively. Also shown are the mean values for 1 bar data. A one-to-one correlation line is shown. The statistics given are for the regression of mean predicted vs measured pressures. For the 1 bar to 16 kbar portion of the data R and SEE for P1 are 1.00 and 0.26 kbar respectively; for model P2 R and SEE are 1.00 and 0.29 kbar. The 1 bar data are from Bender et al. (1984), Grove and Juster (1989), Grove et al. (1992), Juster et al. (1989), Sack and Carmichael (1984), Sack et al. (1987), and Tormey et al. (1987). Also included are unpublished 1 bar data from John Longhi and Rosamond Kinzler. The standard deviations (in kbar) for model P1 (A) are as follows: 1 bar, 2.3; 8 kbar, 1.0; 10 kbar, 2.2; 11 kbar, 0.7; 12 kbar, 2.0; 13 kbar, 0.9; 15 kbar, 2.8; 16 kbar, 1.5; 20 kbar, 2.6; 25 kbar, 4.8

inaccuracy in the model although precision of the estimates cannot be better than the $\pm$ 0.5 kbar quoted for the two model studies. Temperature uncertainties are more difficult to asses because experimental T errors are vulnerable to cryptic difficulties like thermocouple placement shifts, wire batch differences, and contamination. Even so, little evidence exists to suggest T inaccuracies in the models more serious than the quoted experimental precision of $\pm$ 10°C. And yet SEEs of the models (1.36–1.51) are clearly larger than the $P-T$ uncertainties of the model input data. Thus, uncertainties are introduced from a combination of either analytical uncertainty in necessary pyroxene and liquid compositions or from failure to achieve reproducible equilibrium among the phases, no matter how accurately they are analyzed. The analytical strategy of choosing pyroxene rim compositions is common to both model studies. The strategy of Kinzler and Grove (1992) is to average a large number of pyroxene analyses (usually >10) which include some core compositions. As already noted, their data fall within the SEE of the models (see 11, 13 and 16 kbar in Figs. 3 and 4). Except where noted, error on P-predictions from other labs is normally distributed about mean values that are identical to measured pressure. Propagation of compositional analytical imprecision through the model shows that this source of noise accounts for only about $\pm$ 0.5 kbar of error, and is thus an inadequate source for the size of the model SEE. Since the residuals from regression analysis of the models are uncorrelated with P, T, or composition, it is concluded that disequilibrium pyroxene compositions are the most significant source of experimental error.

1 *bar*

One bar data were not incorporated into the thermobarometers and thus provide a test of how well the models extrapolate to pressures below the calibration range. The mean of the estimates (0.09 kbar) is quite close to 1 bar with a standard deviation of 2.3 kbar and a standard error of 0.3 kbar. Predictability of 1 bar data was found to be study-dependent. Some individual studies yield mean estimates that are consistently and significantly higher than 1 bar.

Systematically high pressure estimates in the 1 bar data set probably do not reflect analytical bias (i.e., Na-loss from the glass during microprobe analysis) as this error was not observed in the 8–25 kbar data. Possible sources of error for the 1 bar data may involve the following, (1) Na-loss by volatilization may occur during long runs, especially if the sample size/surface area ratio is small (see Tormey et al. 1987). Although no continuous correlation between run time and error on the pressure estimates exists, all experiments that exceed 500 h in length yield high predicted pressures. Reasonable estimates are also obtained in studies where efforts were made to minimize Na-loss. (2) All experiments run at $T<1050°$ C have negative pressure estimates. The near-solidus temperatures required for pyroxene saturation at 1 bar may lead to sluggish diffusion rates, although it is unclear why this sort of error should be systematic. (3) Sector-zoning is a ubiquitous feature of 1 bar experiments, but is undetected in the near-liquidus experiments of this study. The equilibrium pyroxene composition is obscure when sector-zoning is present.

Prediction of thermodynamic properties

The coefficients derived from regression analysis of Eqs 6 and 11 may be simply related to known thermodynamic quantities. The 1 bar values for H_v^{Di} and H_f^{Di} (enthalpy of vitrification and fusion respectively) and H_v^{Jd} (Navrotsky 1981) were used to test thermodynamic quantities recovered from the models. Comparisons are made at either 1573 or 1600 K since the median and mean of experimental data used in the models (1573 and 1602 K respectively) are in this range. H_f^{Jd} is inferred from H_v^{Jd} assuming that the ratio H_f/H_v is the same for jadeite and diopside. The inferred value of H_f^{Jd} compares well with that recovered from models P1 and P2 (Table 1). The entropy of fusion, S_f^{Jd}, from model P2 also compares well with S_f^{Jd} calculated from C_p and entropy data of jadeite glass (Richet et al. 1993). The volume of fusion, V_f^{Jd}, recovered from model P2 ($V_f^{Jd} = 23.4$ cm^3/mol) is similar to and bracketed by estimates derived from the molar volume of jadeite (Robie et al. 1979) combined with estimates of liquid partial molar volumes (Lange and Carmichael 1987; $V_f^{Jd} = 23.5$ cm^3/mol) and the molar volume of jadeite glass (83.16 cm^3/mol reported by Richet et al. 1993; $V_f^{Jd} = 22.7$ cm^3/mol).

Thermometers

The data set of this study was explored to determine if pyroxene-liquid exchange equilibria involving Mg and Fe would provide a practical geothermometer. Functions analogous to the olivine-liquid equilibria of Roeder and Emslie (1970, Eqs. 11, 12 and 13) were formulated for pyroxene-liquid equilibria but were not nearly as successful as the DiHd-Jd exchange of Eq. 2. Equilibrium 2 was calibrated as a geothermometer (models T1 and T2 in Table 5) using the data of this study combined with the Walter and Presnall (1994) data and randomly selected 1 bar data. The DiHd-Jd exchange equilibrium is also sensitive to pressure, although the volume change of this exchange equilibrium is much smaller than for Jd formation (Table 1). Thermometer T2 incorporates an empirical pressure term. Addition of this pressure term reduces the SEE from 27 to 24 K. The DiHd-CaTs equilibrium of Eq 3 was also calibrated as a thermometer (models T3 and T4 in Table 5); T4 incorporates an empirical pressure term. The use of 1 bar data in models T1 to T4 takes advantage of the wide temperature and bulk-composition ranges spanned by these experiments. The smaller number of data regressed for models T3 and T4 (93 vs 105 for models T1 and T2) reflects the loss of 1 bar data where Al^{VI} in excess of the amount necessary to form jadeite did not exist (i.e., CaTs = 0).

The compositional variable $MgO^{liq}/(MgO^{liq} + FeO^{liq})$ (or $Mg^{\#}$) effectively reduces thermometric error. Thermometers are also improved by adding the compositional variables CaO^{liq} and $AlO_{3/2}^{liq}$ for the respective equilibria K[DiHd-Jd] and K[DiHd-CaTs]. As discussed above, the compositional variables may be treated as activity-modifying terms and are thus presented as $\ln(X_i)$ (Table 5).

Predicting experimental data and thermodynamic properties

Figure 5 shows the temperatures predicted for the regression data for models T1 to T4. Models T1 and T2 (using K[DiHd-Jd]) are somewhat better than models T3 and T4 (using K[DiHd-CaTs]) based on slope and intercept values of predicted vs measured temperature. The SEEs for predictions of the test data are 40 and 30 K respectively for the pressure-independent (T1 and T3) and pressure-dependent (T2 and T4) models. The pressure-dependent models are thus slightly more accurate. The ability of model T2 to recover temperatures of the test data is shown in Fig. 6.

Since most experiments are performed at similar target pressures, the test data may be conveniently grouped into isobaric data sets. Target temperatures are much more variable (as can be seen by comparing the distribution of data in Figs. 3 and 6) and only a small portion of the test data can be grouped into isothermal data sets containing more than 4 or 5 samples. Isothermal separation of the data thus provides an inadequate testing procedure. We can, however, determine the averaging effects on error by predicting both T and P simultaneously. Pressure predictions for the test data in Fig. 4A utilize measured experimental temperatures (recall that barometer P1 is temperature-sensitive). Figure 7 alternatively shows the mean of pressure estimates from model P1 when temperatures are estimated with model T1. These P-estimates are thus derived using only compositional information. Figure 7 gives a measure of the total error when models P1 and T1 are used in combination, as would be the case with natural samples when only compositional information is available. Mean values of P-estimates calculated by this method may be compared to the mean values calculated with reported temperatures (compare Fig. 7 to Fig. 4A). The SEE on the mean values increases from 0.3 to 0.8 kbar on the 1 bar–16 kbar portion of the test data. This 0.5 kbar increase in SEE may be attributed to the error introduced by the temperature-estimate from model T1, which corresponds to an average error of about 15 K over the amount of error inherent in model P1.

Application to basalts from Hawaii

Many basaltic rocks lie on low-pressure differentiation trends suggesting crystallization at shallow levels in the

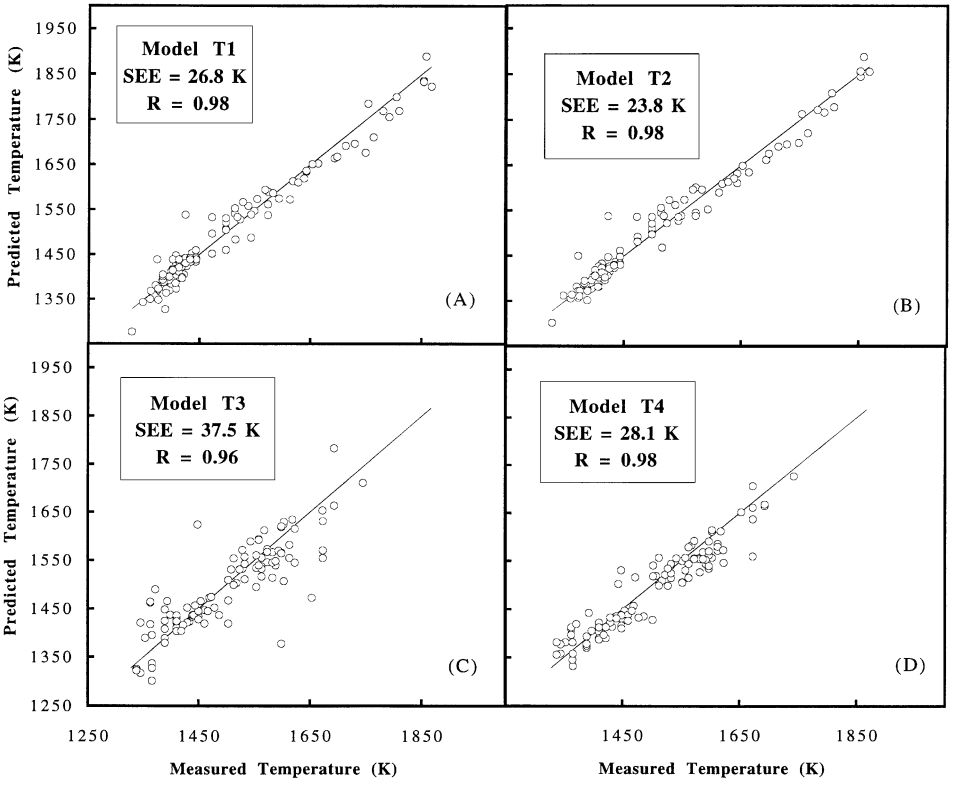

Fig. 5A–D Temperatures are recovered for the data used in the regressions. One-to-one correlation lines and statistics on model regressions are given in each figure. **A** and **B** compare the *P*-independent and P-dependent models T1 and T2 respectively, both of which are based on DiHd-Jd exchange. **C** and **D** compare the DiHd-CaTs-based models T3 and T4, which are *P*-independent and *P*-dependent respectively. The data used to form the models are identical to those used to form the thermobarometers with additional 1 bar data selected from the following studies: Grove et al. (1992), Juster et al. (1989), Sack et al. (1987), Tormey et al. (1987) and unpublished data from Rosamond Kinzler

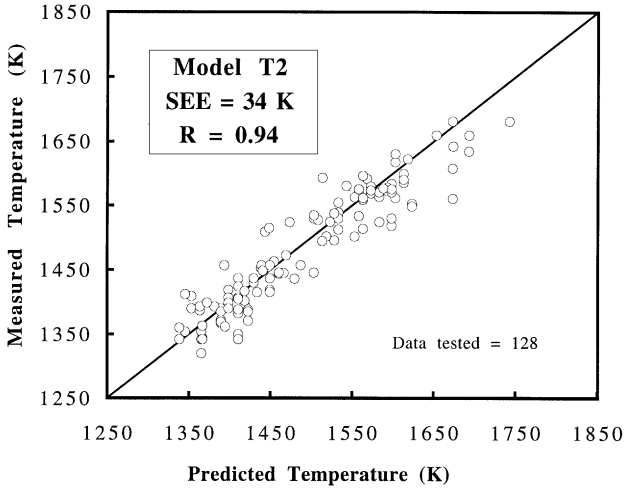

Fig. 6 Model T2 is used to predict temperatures of the test data. The line shown is a one-to-one correlation line. A regression of measured vs predicted temperatures yields a slope of 0.99 and a zero intercept of 17 K; the SEE and R are shown. The sources of the high pressure portion of the test data are the same as those used in Fig. 3. 1 bar data were selected from the sources listed in Fig. 5 and chosen so that the test and model data sets do not overlap

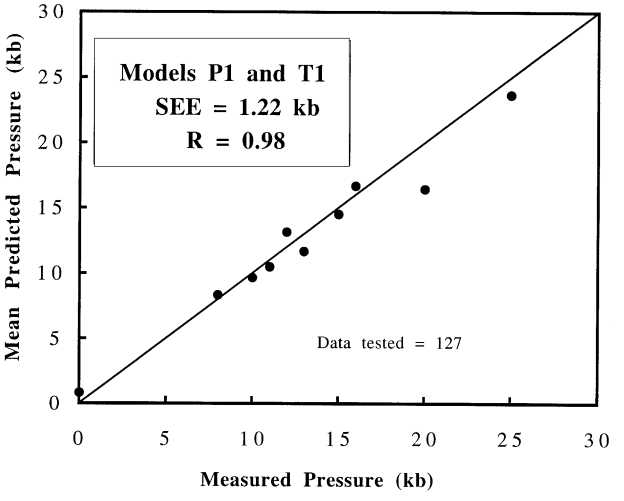

Fig. 7 Mean values of predicted pressures are shown for the same data used to construct Fig. 3 and 4. Model T1 is used to estimate temperature. This temperature estimate, instead of the measured temperature, is then used in model P1 to estimate pressure. Statistics for the 1 bar–25 kbar data (mean predicted vs measured) are shown; a regression through the data from 1 bar to 16 kbar give an R of 1.00 and an SEE of 0.8 kbar with a slope of 0.99 and an intercept of 0.06 kbar. Compare Fig. 4A

lithosphere. Some basalts, however, may bypass shallow level storage chambers and erupt directly from greater depths. Phenocryst compositions may record these depths and may be used to calculate and compare such transport depths from one volcanic suite or tectonic environment to another.

We apply our thermobarometers to the problem of transport depth by examining pyroxene and whole-rock host compositions from Mauna Kea, Hawaii (Frey et al. 1991). Depth-estimates are then compared

to estimates of elastic plate thickness and depth to seismic activity beneath Hawaii to infer controls on magma transport. $P-T$ estimates are compared to trace-element geochemistry to constrain magma genesis.

The compositional data (Frey et al. 1991) consist of pyroxene rim and core compositions and whole-rock analyses. The rocks include post-shield ankaramites of alkalic affinity (MU-9 and LP-5), post-shield tholeiitic basalts (MU-2 and MU-8), a post shield high Fe–Ti basalt (KI-12), and submarine shield tholeiites (MK1-8 and MK6-18). Together these basalts represent a phase transitional between shield-building tholeiitic and post-shield alkalic volcanism. To estimate pressure and temperature (Fig. 8) model P1 was solved simultaneously with model T2.

Testing for closed system behavior

We first checked whether reported whole-rock compositions can represent a liquid from which phenocryst pyroxenes crystallized. Comparing olivine and host whole-rock compositions allowed an initial check that whole-rock compositions potentially represent a liquid. We compare measured versus model K_D^{ol-liq}[Mg–Fe] ($[FeO^{ol}*MgO^{liq}]/[FeO^{liq}*MgO^{ol}]$). The Roeder and Emslie (1970) model, based on experiments on basaltic bulk-compositions at 1 bar, demonstrates a constant value for K_D^{ol-liq}[Mg–Fe] of 0.30 $\pm$ 0.03. We performed a multiple linear regression on 190 olivine-liquid pairs synthesized between 1 bar and 100 kbar. The regression equation used was a variation of Eq. 5. We found compositional dependencies similar to those noted by Gee and Sack (1988) and Langmuir et al. (1992) as well as a slight P/T dependency that is consistent with the anticipated ΔV_r for the exchange equilibrium (1.5 cm^3/mol). The resulting function is

$$\ln K_D^{ol-liq}[\text{Mg–Fe}] = -1.87 + \frac{11.07*P}{T} + 1.67*[SiO_2^{liq}] - 14.11*[Na^{liq}*Al^{liq}] \quad (13)$$

where P is in kbar and T is in Kelvin (Fig. 9). Applying our model to whole-rock compositions from Hawaii over a range of pressures (0–20 kbar) indicates that equilibrium olivines crystallizing from whole-rock compositions should yield $K_D^{ol/whole\text{-}rk}$[Mg-Fe] = 0.30 for all samples. Use of the Sack et al. (1980) model for estimating ferric/ferrous ratios for an ankaramite whole-rock composition (MU-8) also shows that substantial deviation (16% error) of K_D^{ol-liq}[Mg–Fe] from 0.3 will occur for such samples only if oxygen fugacities approach Ni-NiO.

Only one sample for which $P-T$ estimation was attempted, MU-9, showed a large discrepancy between the observed and expected value of $K_D^{ol/whole-rk}$[Mg–Fe]. Olivine compositions from MU-9 yield an average $K_D^{ol/whole-rk}$[Mg–Fe] of 0.42. Since this value is significantly higher than 0.30, the whole-rock composition was corrected by subtracting olivine of an average core composition until $K_D^{ol/whole-rk}$[Mg–Fe] = 0.30; the amount of olivine removed (6%) does not exceed the

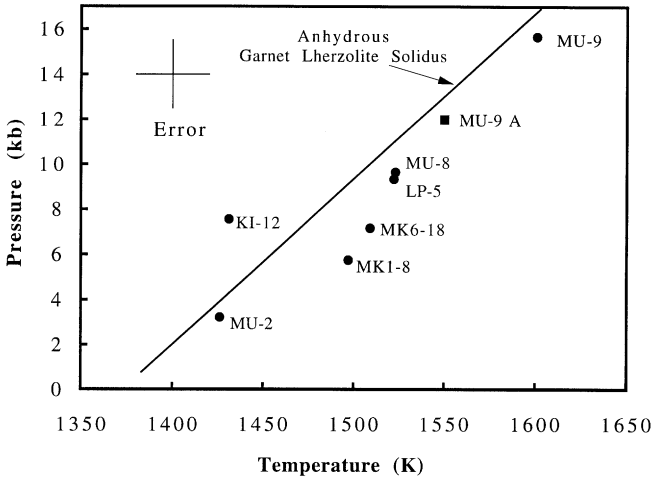

Fig. 8 Model P1 is used in combination with model T2 to estimate the pressure and temperature of pyroxene-bulk rock pairs from data reported by Frey et al. (1991). Also illustrated is the mantle solidus of McKenzie and Bickle (1988). Sample numbers are from Frey et al. (1991). Samples MU-9 and LP-5 are postshield ankaramites. Samples MU-2 and MU-8 are postshield tholeiitic basalts. Samples MK1-8 and MK6-18 are submarine shield tholeiites. Sample KI-12 is a postshield high Fe-Ti basalt. "MU-9 A" represents the $P-T$ estimate for MU-9 after compositional corrections were made; see text for explanation. Error bars in upper left corner

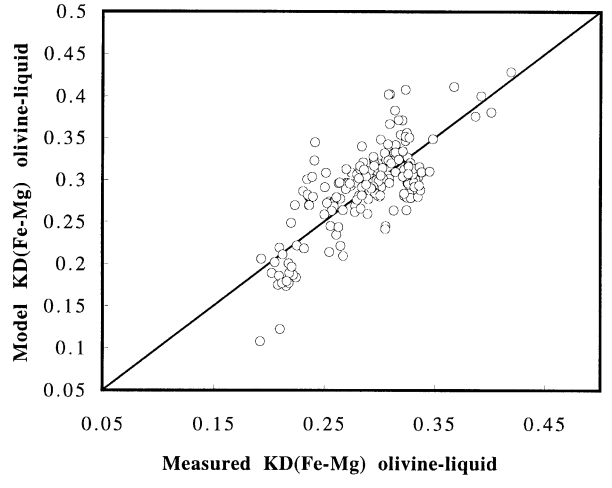

Fig. 9 Measured values of K_D^{ol-liq}[Mg–Fe] are plotted against values of K_D^{ol-liq}[Mg–Fe] predicted from Eq. 13. The model SEE is 0.03 and the correlation coefficient is 0.75. The model is based on experimental equilibrium olivine-liquid pairs from: Gee and Sack (1988), Longhi and Pan (1988), Falloon and Green (1987), Bender et al. (1984), Kinzler and Grove (1992), Takahashi (1986), Grove et al. (1992), Sack et al. (1987), and Tormey et al. (1987). Also included are unpublished data from Rosamond Kinzler

modal amount of olivine. The resulting $P - T$ estimate is 12 kbar and 1550 K (40 km and 1277° C). This 'adjusted' $P - T$ estimate is shown in Fig. 8 as MU-9 A, and is much nearer to $P - T$ estimates for samples LP-5 and MU-8. No corrections were made for the remaining samples. Notably, all samples except KI-12, plot to the high-temperature side of the anhydrous garnet peridotite mantle solidus of McKenzie and Bickle (1988). Thus the $P - T$ solutions seem physically reasonable. Frey et al. (1991) presented evidence for disequilibrium between phenocrysts and whole-rock for sample KI-12; this sample is probably not amenable to a simple corrective scheme. Disequilibrium may be the reason sample KI-12 does not plot on an otherwise coherent $P - T$ trend.

Petrological implications

Where in the mantle and by what processes do alkalic and tholeiitic rocks gain their characteristics? Thermobarometers may provide constraints. Sample MU-8 is argued by Frey et al. (1991) to be the "the best example of a parental tholeiitic melt" while sample LP-5 is considered "clearly related to the alkalic lavas" (due to comparatively high La/Yb and Zr/Nb).

$P - T$ estimates (based on core compositions and whole-rock analyses) for LP-5 and MU-8 are identical within model error. Interestingly, use of pyroxene rim compositions for both samples results in P-estimates identical to those based on pyroxene cores (the whole-rock composition of LP-5 is corrected for pyroxene crystallization when pyroxene rims are used in the model; MU-8 is 98.5% glass). Temperature-estimates from rims and cores are also identical for MU-8 and LP-5; the thermometer is insensitive to the small variations in temperature with the existing data set. Since pyroxene saturation occurs at lower temperatures for lower pressures we might expect re-solution of pyroxenes rather than growth during upward adiabatic transport, thus, similar P-estimates using rim and core compositions are not surprising. Rims yielding lower P-estimates may occur if magma stalls at shallow depths, but time of stagnation must be long enough for temperature to fall and for pyroxene to become re-saturated (as possibly occurred for MU-2 (93.2% glass); $P - T$ estimates for MU-2 are 3.2 kbar and 1426 K using the core composition, and 0.06 kbar and 1402 K using the rim). We suspect that pyroxenes in MU-8 and LP-5 experienced most of their growth at a single depth and were transported to the surface with insufficient time for significant growth and/or re-equilibration. A combined average taken from core and rim compositions from both LP-5 and MU-8 likely provides the best $P - T$ estimate. Calculated in this way the mean P and T estimates (with standard deviations) are: 10.2 ± 0.8 kbar and 1530 ± 7.0 K (about 34 km at 1257° C; assume 3.3 km/kbar). Direct transport for these samples from 34 km without further stagnation and petrogenetic activity is thus indicated.

These parental tholeiite (MU-8) and alkalic basalts (LP-5) have identical SiO_2, TiO_2 and CaO/Al_2O_3, and have similar $Mg^{\#}$s (61 and 63 respectively). This observation and the similar P-estimates for these samples suggest that trace- and alkali-element contents are established below depths of 34 km. Clague (1987) has hypothesized the existence of a magma storage zone at 20 km (the base of the crust) based on xenolith populations. Our P estimates are consistent with a deep level of stagnation, but place this ponding level at a depth greater than 20 km.

Comparisons to geophysical data

Controls upon magma transport may be inferred by comparing pressure and corresponding depth estimates to seismic data. The maximum depth-estimate (40 km assuming 3.3 km/kbar) for lavas from Mauna Kea corresponds to depths inferred for magma-related tremor (Aki and Koyanagi 1981) and a low velocity zone beneath Hawaii (Ryan 1988) and thus, unsurprisingly, relate such seismic phenomena to the presence of melt at these depths.

All magma transport depths, except MU-2, exceed depth estimates for the base of the crust (18 km; Hill and Zucca 1987). Also, Hill and Zucca (1987) infer a density for the lower crust of 2.9 g/cm^3; the base of the crust does not provide a level of neutral buoyancy for basaltic magma with a density = 2.7 g/cm^3. The range of depth estimates, however, has a shallow bound that roughly coincides with the long-term elastic thickness (T_e) of the lithosphere (25 km; Watts et al. 1985). Depths for extraction of magma may thus be sensitive to the mechanical behavior of the lithosphere. For appropriate mantle strain rates (10^{-14}–10^{-18}/s) the elastic thickness may represent the depth of ductile behavior and a sharp decrease in strength (Kirby 1980; Bodine et al. 1981). The match of the lower limit of depth estimates with T_e suggests that magma transport is controlled, through temperature, by the depth to the brittle-ductile transition, and further implies a similar control for both fracture propagation and long-term lithospheric strength.

When P-T estimates are obtained from other volcanoes and combined with age constraints, both petrologic models and comparisons to geophysical data can be further refined. Application of the thermobarometers to rocks from Mauna Kea nevertheless demonstrate (1) the use of thermobarometry in constraining the origin of alkalic vs tholeiitic magma, (2) that magma may be delivered to a planetary surface from substantial depth and (3) ponding of magma may be controlled by the elastic thickness of the lithosphere.

Summary

New experiments in the range 8 to 30 kbar produced clinopyroxene-liquid pairs whose compositional systematics were used to construct various geothermobarometers. These expressions have a thermodynamic basis and thermodynamic properties can be calculated from coefficients of the expressions. These thermodynamic properties, $\Delta H_r^{P_0}$, $\Delta S_r^{P_0}$ and ΔV_r, have values similar to 1 bar literature values. As expected, the Jd-liq equilibrium, which has a high ΔV_r, proved to be the basis of a useful geobarometer. Exchange equilibria involving solution of Jd and CaTs into DiHd are less sensitive to pressure and were calibrated as thermometers.

The thermobarometric models reliably reproduced pressures and temperatures of experiments from other labs. Error analysis indicates that P and T estimates using the preferred models, P1 and T1, (Table 5) are accurate to at least $\pm$ 1.4 kbar and $\pm$ 27 K on individual pyroxene/liquid pairs, and perhaps as good as $\pm$ 1.0 kbar and $\pm$ 15 K when averages over multiple equilibrium pyroxene/liquid pairs are used. The pressure-dependent thermometer, T2, (Table 5) may provide more accurate estimates. Since test and model data encompass a wide range of bulk compositions, the thermobarometers should be generally applicable to mafic igneous rock compositions.

Application of the models to rocks from Mauna Kea, Hawaii yield transport depths up to 40 km for ankaramites. Also, samples MU-8, a parental tholeiite (Frey et al. 1991) and LP-5, a parental alkalic basalt, yield identical pressure-estimates (10.2 kbar). The similar pressure estimates, but different trace-element contents for these samples, indicate that tholeiitic and alkalic volcanic rocks at Hawaii inherit their trace-element signatures below 34 km. The agreement of maximum depth-estimates for mafic rocks from Hawaii with depths observed for tremors and the low velocity zone suggest that volcanic rocks may be delivered from substantial depths without significant re-equilibration of liquid and coexisting pyroxene. Depth estimates also have a shallow bound that corresponds to elastic plate thickness. This indicates that the mechanical behavior of the lithosphere, not density contrasts, controls magma storage at depth below Hawaii. This latter observation implies the utility of igneous thermobarometry not only towards disentangling problems of petrogenesis but also regarding tectonic issues.

Acknowledgements We thank Barbara Molfino for advice concerning statistical matters. Comments by, and discussions with Charlie Langmuir, George Harlow and Robert Fogel were extremely helpful as were discussions with Daniel Farber, Mark Davis and Jennifer Reynolds. The manuscript was improved from reviews by Michael Walter and Roger Nielsen. The ankaramite, ugandite and Mid-Atlantic ridge basalt samples used as starting compositions were generously donated by Fred Frey, Richard Sack and Jennifer Reynolds respectively. Electron microprobe work was greatly facilitated by Linnea Norby. Numbers of experiments were carefully and thoughtfully counted by Noelani Putirka. Supported by grants from NSF and DOE. LDEO contribution #5410.

References

Aki K, Koyanagi R (1981) Deep volcanic tremor and magma ascent mechanism under Kilauea, Hawaii. J Geophys Res 86: 7095–7109

Bartels KS, Kinzler RJ, Grove TL (1991) High pressure phase relations of primitive high-alumina basalts from Medicine Lake volcano, northern California. Contrib Mineral Petrol 108: 253–270

Bender JF, Langmuir CH, Hanson GN (1984) Petrogenesis of basalt glasses from the Tamayo Region, East Pacific Rise. J Petrol 25: 213–254

Bodine JH, Steckler MS, Watts AB (1981) Observations of flexure and the rheology of the oceanic lithosphere. J Geophys Res 86: 3695–3707

Bottinga Y, Weill DF (1972) The viscosity of magmatic silicate liquids: a model for calculation. Am J Sci 272: 438–475

Clague DA (1987) Hawaiian xenolith populations, magma supply rates, and development of magma chambers. Bull Volcanol 49: 577–587

Drake MJ (1976) Plagioclase-melt equilibria. Geochim Cosmochim Acta 40: 457–465

Elthon D, Scarfe CM (1984) High-pressure phase equilibria of a high-magnesia basalt and the genesis of primary oceanic basalts. Am Mineral 69: 1–15

Falloon TJ, Green DH (1987) Anhydrous partial melting of MORB pyrolite and other peridotite compositions at 10 kbar: implications for the origin of primitive MORB glasses. Mineral Petrol 37: 181–219

Fram MS, Longhi J (1992) Phase equilibria of dikes associated with Proterozoic anorthosite complexes. Am Mineral 77: 605–616

Frey FA, Garcia MO, Wise WS, Kennedy A, Gurriet P, Albarede F (1991) The evolution of Mauna Kea Volcano, Hawaii: petrogenesis of tholeiitic and alkalic basalts. J Geophys Res 96: 14347–14375

Gee LL, Sack R (1988) Experimental petrology of melilite nephelinites. J Petrol 29: 1233–1255

Ghiorso MS, Carmichael ISE, Rivers ML, Sack RO (1983) The Gibbs free energy of mixing of natural silicate liquids; an expanded regular solution approximation for the calculation of magmatic intensive variables. Contrib Mineral Petrol 84: 107–145

Grove TL, Juster TC (1989) Experimental investigations of low-Ca pyroxene stability and olivine-pyroxene-liquid equilibria at 1-atm in natural basaltic and andesitic liquids. Contrib Mineral Petrol 103: 287–305

Grove TL, Kinzler RJ, Bryan WB (1992) Fractionation of mid-ocean ridge basalt (MORB). Geophys Monogr Am Geophys Union 71: 281–310

Hill DP, Zucca JJ (1987) Geophysical constraints on the structure of Kilauea and Mauna Loa volcanoes and some implications for seismomagmatic processes. US Geol Surv Prof Pap 1350: 903–917

Juster TC, Grove TL, Perfit MR (1989) Experimental constraints on the generation of FeTi basalts, andesites and rhyodacites at the Galapagos Spreading center, 85°W and 95°W. J Geophys Res 94: 9251–9274

Kinzler RJ, Grove TL (1992) Primary magmas of mid-ocean ridge basalts 1. Experiments and methods. J Geophys Res 97: 6885–6906

Kirby SH (1980) Tectonic stresses in the lithosphere: constraints provided by the experimental deformation of rocks. J Geophys Res 85: 6353–6363

Lange RA, Carmichael ISE (1987) Densities of Na_2O–nK_2O–CaO–MgO–FeO–Fe_2O_3–Al_2O_3–TiO_2–SiO_2 liquids: new measurements and derived partial molar properties. Geochim Cosmochim Acta 51:2931–2946

Langmuir CH, Klein EM, Plank T (1992) Petrological systematics of mid-ocean ridge basalts: constraints on melt generation beneath ocean ridges. Geophys Monogr Am Geophys Union 71:183–280

Lindsley DH (1983) Pyroxene thermometry. Am Mineral 68: 477–493

Longhi J, Pan V (1988) A reconnaisance study of phase boundaries in low-alkali basaltic liquids. J Petrol 29:115–147

McKenzie D, Bickle MJ (1988) The volume and composition of melt generated by extension of the lithosphere. J Petrol 29:625–679

Navrotsky A (1981) Thermodynamics of mixing in silicate glasses and melts. In: Newton RC, Navrotsky A, Wood BJ (eds) Thermodynamics of minerals and melts, Springer New York, pp 189–206

Nielsen RL, Drake MJ (1979) Pyroxene-melt equilibria. Geochim Cosmochim Acta 43:1259–1272

Perfit MR, Langmuir CH, Baekisapa M, Chappell B, Johnson RW, Staudigel H (1987) Geochemistry and petrology of volcanic rocks from the Woodlark Basin: addressing questions of ridge subduction. In: Taylor B, Exon NF (eds) Marine Geology, geophysics, and geochemistry of the Woodlark Basin-Solomon Islands. Circum Pacific Council for Energy and Mineral Resources, Earth Sci Series 7, Houston Texas, pp 113–154

Richet P, Robie RA, Hemingway BS (1993) Entropy and structure of silicate glasses and melts. Geochim Cosmochim Acta 57: 2751–2766

Robie RA, Hemingway BS, Fisher JR (1979) Thermodynamic properties of minerals and related substances at 298.15 K and 1 bar (10^5 Pascals) pressure and at higher temperatures. US Geol Surv Bull 1452:456

Roeder PL, Emslie RF (1970) Olivine-liquid equilibrium. Contrib Mineral Petrol 29:275–289

Ryan MP (1988) The mechanics and three-dimensional internal structure of active magmatic systems: Kilauea volcano, Hawaii. J Geophys Res 93:4213–4248

Sack RO, Carmichael ISE (1984) $Fe^2 = Mg^2$ and $TiAl_2 = MgSi_2$ exchange reactions between clinopyroxenes and silicate melts. Contrib Mineral Petrol 85:103–115

Sack RO, Carmichael ISE, Rivers M, Ghiorso MS (1980) Ferric-ferrous equilibria in natural silicate liquids at 1 bar. Contrib Mineral Petrol 75:369–376

Sack RO, Walker D, Carmichael ISE (1987) Experimental petrology of alkalic lavas: constraints on cotectics of multiple saturation in natural basic liquids. Contrib Mineral Petrol 96:1–23

Stebbins JF, Carmichael ISE, Moret LK (1984) Heat capacities and entropies of silicate liquids and glasses. Contrib Mineral Petrol 86:131–148

Takahashi E (1986) Melting of a dry peridotite KLB-1 up to 14 GPa: implications on the origin of peridotitic upper mantle. J Geophys Res 91:9367–9382

Tormey DR, Grove TL, Bryan WB (1987) Experimental petrology of normal MORB near the Kane Fracture Zone: 22°–25° N, mid-Atlantic Ridge. Contrib Mineral Petrol 96:121–139

Walter MJ, Presnall D (1994) Melting behavior of simplified lherzolite in the system CaO-MgO-Al_2O_3-SiO_2-Na_2O from 7 to 35 kbar. J Petrol 35:329–359

Watts AB, ten Brink US, Buhl P, Brocher TM (1985) A multichannel seismic study of lithosphereic flexure across the Hawaiian–Emperor seamount chain. Nature 315:105–111

Zhang Y, Walker D, Lesher CE (1989) Diffusive crystal dissolution. Contrib Mineral Petrol 102:492–513